# Nanotribology: friction, wear and lubrication at the atomic scale

**Bharat Bhushan, Jacob N. Israelachvili & Uzi Landman**

**Friction, wear and lubrication between materials in contact are of fundamental importance in many pure and applied sciences. Owing to the development of experimental and computer-simulation techniques for studying these phenomena at the atomic scale, an understanding is beginning to emerge of the molecular mechanisms of tribology in thin films and at surfaces.**

UNDERSTANDING the atomic processes occurring at the interface of two materials when they are brought together, separated or moved with respect to one another is central to many technological problems, including adhesion, contact formation, friction, wear, lubrication, nanoindentation, fracture and machining[1–4]. At most interfaces of technological relevance, contact occurs at numerous asperities[1,2]. Consequently, the importance of investigating single asperity contacts in studies of the fundamental micromechanical and tribological properties of surfaces and interfaces has been long recognized[5–14]. The recent emergence and proliferation of proximal probes, in particular tip-based microscopies (the scanning tunnelling microscope and the atomic-force microscope) and the surface-force apparatus, and of computational techniques for simulating tip–surface interactions and interfacial properties, has allowed systematic investigations of interfacial problems with high resolution as well as ways and means for modifying and manipulating nanoscale structures. These advances provide the impetus for research aimed at developing a fundamental understanding of the nature and consequences of the interactions between materials on the atomic scale, and they guide the rational design of materials for technological applications. In short, they have led to the appearance of the new field of nanotribology[15,16], which pertains to experimental and theoretical investigations of interfacial processes on scales ranging from the atomic and molecular to the microscale.

The surface-force apparatus (SFA)[17–24], the scanning tunnelling microscope (STM)[25], the atomic-force and friction-force microscopes (AFM and FFM)[26–28], as well as the quartz microbalance technique[29], are widely used in nanotribological studies. The SFA was developed in the late 1960s and is commonly employed to study both static and dynamic properties of molecularly thin films sandwiched between two molecularly smooth surfaces. The STM, developed in 1981, allows imaging of electrically conducting surfaces with atomic resolution, and has been used for imaging of clean surfaces as well as of lubricant molecules. The introduction of the atomic-force microscope in 1985 provided a method for measuring ultra-small forces between a probe tip and an electrically conducting or insulating surface, and has been used for topographical measurements of surfaces on the nanoscale, as well as for adhesion and electrostatic fore measurements. Subsequent modifications of the AFM led to the development of the friction-force microscope (FFM), designed for atomic-scale and microscale studies of friction. This instrument measures forces transverse to the surface. The AFM is also being used for investigations of wear, indentation, detection of transfer of material, boundary lubrication, and nanofabrication and machining. Meanwhile, significant progress in understanding the fundamental nature of bonding and interactions in materials, combined with advances in computer-based modelling and simulation methods, have allowed theoretical studies of complex interfacial phenomena with high resolution in space and time[15,16]. Such simulations provide insights into atomic-scale energetics, structure, dynamics, thermodynamics, transport and rheological aspects of tribological processes. Furthermore, these theoretical approaches guide the interpretation of experimental data and the design of new experiments, provide a framework for analysis and development of unifying concepts, and enable the prediction of new phenomena based on atomistic principles.

Here we review several of the principal theoretical and experimental aspects of research in nanotribology. The nature of interactions between two surfaces brought close together, and those between two surfaces in contact as they are separated, have been studied experimentally with the surface-force apparatus. This has led to a basic understanding of the normal forces between surfaces, and of the dramatic way in which these are modified by the presence of an intervening medium such as a liquid or a polymer 'brush' adsorbed or chemically grafted to the surfaces. The frictional properties of such systems have been studied by moving the surfaces laterally, and such experiments have provided insights into the molecular-scale operation of lubricants such as thin liquid or polymer films. Often, these lubricants behave in ways that would not be predicted on the basis of their bulk-scale behaviour alone.

Complementary to these studies are those in which the AFM and FFM are used as a 'model asperity' in contact with a solid surface. These experiments have demonstrated that the relationship between friction and surface topography is not always simple or obvious. AFM studies have also revealed much about the nanoscale nature of intimate contact—of indentation and wear. Computer simulations of tip–surface interactions at the atomic scale have shown the surface need not behave as an elastic medium but can deform plastically, for example leading to 'necking' between surface layers and the probe tip.

## Surface-force studies of thin films

The surface-force apparatus has long been used to measure both static[17,19] and dynamic[18,20–24] forces between smooth, macroscopic surfaces. As with AFMs and most other force-measuring devices, forces are determined from the deflection of a spring, and displacements are measured using some optical, electrical, capacitive or strain-gauge technique. The principle of operation of SFAs (Fig. 1) is thus fairly simple; the challenge comes in measuring very weak forces, sub-microscopic surface geometries and surface separations at the ångström level.

**Static (equilibrium) properties of thin liquid films.** The intermolecular interaction potential or force function between two surfaces interacting in or across a liquid medium can be attractive, repulsive, 'oscillatory' or a more complex function of separation. Recent experiments and theoretical studies (mainly computer simulations) have shown that the structure of the liquid molecules and of the confining surfaces are very important in determining what the force function will be[30–45]. Furthermore, two crystalline surfaces may induce a liquid to solidify (freeze) when the gap thickness is close to a small multiple of the molecular diameter (Fig. 1, bottom left)[37–40,46,47]. The oscillatory force-function resulting from such an interaction is illustrated in Fig. 1 (top left)[31–33].

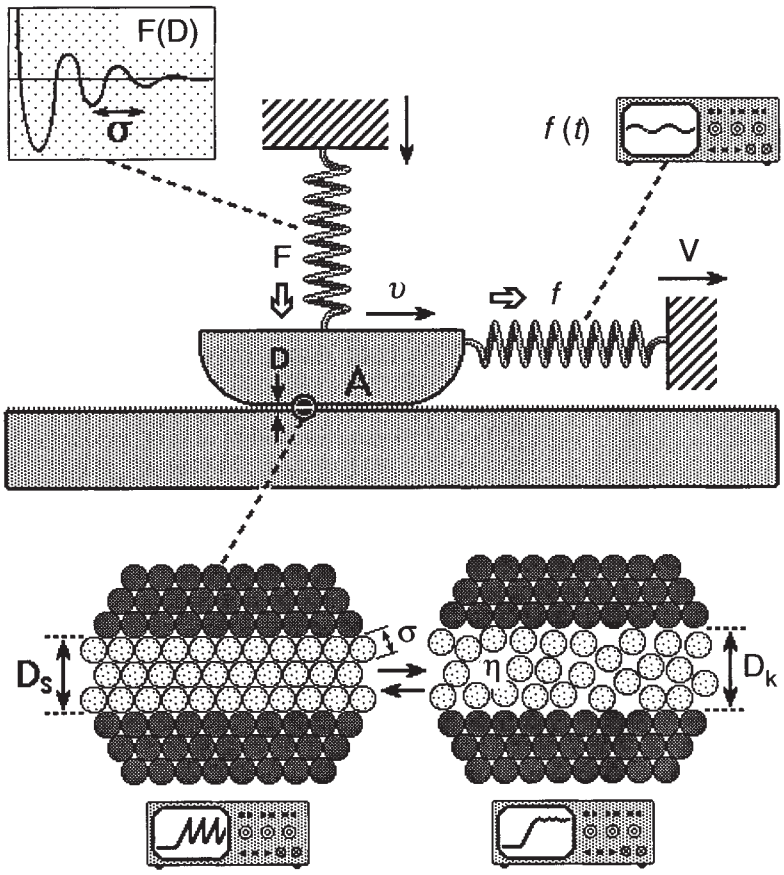


FIG. 1 Illustration of the principle of the surface-force apparatus (SFA) for measuring the normal forces, $F$, and friction or shear forces, $f$, between two smooth surfaces of area $A$ separated by a thin liquid film of thickness $D$ (refs 18–24). An optical interference technique allows the shapes of the surfaces and their separation, $D$, to be accurately monitored during force and friction measurements. Typical contact area $A$ is 100 $\mu m^2$, and gap thicknesses can range from one molecular layer ($D = \sigma = 4$ Å, where $\sigma$ is the molecular diameter) to thousands of ångströms. An oscillatory force-function, $F(D)$, typically measured across simple liquids is shown at top left, and two common types of friction traces (friction force versus time: $f(t)$) are shown in the oscilloscopes at the bottom of the figure. During sliding, two smooth surfaces usually remain in one of the adhesive minima of the force function, although the kinetic film thickness $D_k$ is usually slightly different from the equilibrium or static thickness, $D_s$.

The structure adopted by molecules in ultra-thin films is generally very different from their bulk structure; other thin-film properties may also be very different. The freezing point may be higher or lower, depending on whether the 'epitaxial' interaction of the confined molecules with the two surfaces is cooperative or disruptive[37–40,48] and molecular relaxation times can be many orders of magnitude longer than in the bulk[23,24,47,49–51]. It is also interesting to note that even though one surface can have an effect on the structure of the liquid molecules adjacent to it[33,52–55], the effect of two confining surfaces is generally much more dramatic, and can produce a greater variety of interfacial (non-bulk-like) structures—amorphous, solid or liquid-crystalline—each of which gives rise to a different type of force function as well as to different dynamic properties, as described below.

**Dynamic and shear properties of thin films.** The force between two surfaces across a liquid or lubricant fluid tells us whether two surfaces, when pressed together, will come into adhesive contact or remain separated by a thin, liquid-like layer[30–33,36,56]. This is crucially important for understanding the behaviour that results when one of the surfaces is made to move laterally or to shear past the other, as occurs during frictional and lubricated sliding. For example, if the two surfaces are in true molecular contact when sliding begins, their friction will be high and their adhesion may be strong enough to tear them apart. If, however, the surfaces are separated by one or more molecular layers of the fluid, and if this cushioning film remains in the liquid-like state during sliding, this may ensure that the friction force $f$ will be low and that sliding will proceed smoothly (Fig. 1, bottom right). Experiments have shown that even one layer of water molecules, approximately 0.25 nm thick, between two hydrophilic surfaces can be sufficient to reduce the interfacial friction force to a very low value[57].

On the other hand, if the surface–fluid interactions induce the liquid molecules to solidify, the molecular configuration during sliding will be much more complicated. In such cases the film alternately melts and freezes during the motion[37,40,46,47,58–60], as shown schematically in the lower part of Fig. 1; the resulting friction is of the 'stick–slip' type. Sticking occurs in the frozen state, giving rise to the static friction force, $f_s$, and slipping occurs in the shear-induced molten state, giving rise to the kinetic friction force, $f_k$. The real situation, even for the simplest surfaces and liquids, is actually much more complicated than shown in Fig. 1: the direction of sliding is generally at some angle to the surface lattices, the two surface lattices are not generally in registry, the surface and liquid molecules have different diameters, and they are generally not even spherical. This complexity leads to complex force functions and friction–time relationships. Even for quite complex force functions, however, recent experiments have shown that the forces of friction and adhesion are closely related[61].

**Shear-induced ordering transitions.** Recent experiments and computer simulations have shown that different types of ordered structures may occur during frictional sliding[37–41,62]. The idea of a 'structure' being induced by motion is an unfamiliar concept, but 'shear-induced ordering' is at the heart of what goes on in such thin films. Different types of ordered states can appear depending on the temperature, load and sliding velocity, and dynamic phase transitions between these states can also occur during sliding, each giving rise to a complex stick–slip friction pattern. Such effects are now believed to underlie many other apparently unrelated dynamic processes involving stick–slip motion, such as earthquakes, the sound of a violin (and other instruments), the squeaking of doors, and sensory perception (of touch and even taste)[48].

Figure 2 shows some of the dynamic film structures that can arise during the sliding of two surfaces that contain boundary layers of surfactant molecules. In general, solid-like films exhibit stick–slip motion, amorphous-like films exhibit high friction due to the molecular interdigitations and entanglements occurring between the two surfaces, and liquid-like films exhibit low, viscous-like friction with smooth sliding. These dynamic states are not intrinsic properties of a shearing film (in the way that they are for bulk condensed phases at any given temperature and pressure): they depend not only on the temperature and pressure

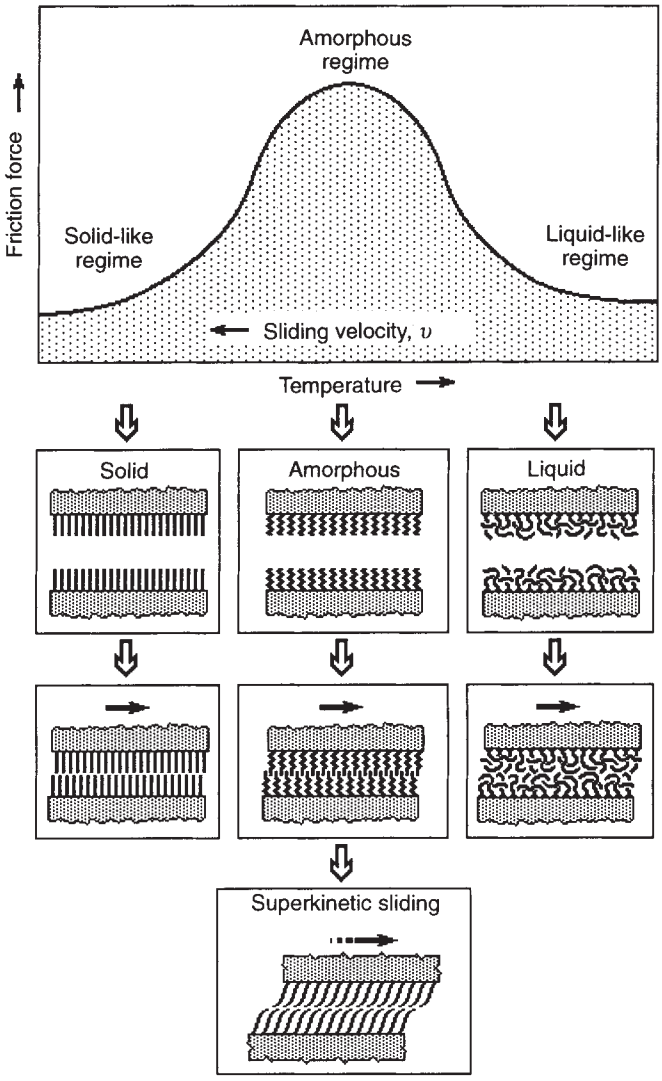


FIG. 2 Schematic illustrations of different types of dynamic thin-film structures that can arise during lubricated sliding. Top, dynamic phase diagram representation of friction force (or rate of energy dissipation) as a function of temperature or sliding velocity (adapted from refs 61 and 62). Under certain favourable conditions involving surface-grafted chain molecules[62], the entangled molecules at the interface may undergo 'shear-induced ordering', when they disentangle and become aligned; at the same time the friction force drops significantly (superkinetic friction).

or applied load, but also on the relative sliding velocity of the two shearing surfaces (which is not necessarily the same at the velocity of the drive: see Fig. 1). Higher sliding speeds make the film more solid-like, whereas slower speeds make it behave more like a liquid. This principle, known as time–temperature superposition, has recently been found to be very useful in understanding the effects of time, temperature, load and other variables on the complex molecular processes occurring at a shearing interface and the resulting friction forces[61].

**Attaining desirable friction properties.** The attainment of low adhesion, low friction and low wear (surface damage) is usually a desirable practical goal. But there are cases where the aim may be to attain a constant friction force (with load or speed) or even a high friction, as occurs in the case of clutch fluids. By judiciously choosing the right lubricant fluid and, in some cases, by chemically grafting chain-like molecules such as surfactants[62] or polymers[63] to surfaces (these are known as boundary lubricants), it is becoming possible to control the frictional properties of moving components in machines and other devices. For example, the grafting of certain surfactant molecules at a certain coverage to surfaces has been found[62] to produce films that can undergo a dynamic first-order transition from a high friction state to a low friction state (Fig. 2). The advantage of such a lubricant system is that no lubricant fluid is actually ever applied or needed—the surfaces are self-lubricating in the sense that they are processed right from the start to carry their own lubricant layer with them; also, very small quantities of material are needed so that material costs should not be prohibitive even for fairly expensive lubricants. This is a good example of how recent research in the field of molecular tribology is opening up possibilities for creating new types of lubricant systems.

## AFM/FFM studies of tribological processes

Adhesion[64–68], friction[27,28,69–77], wear[71–73,76–78] and lubrication[64,79–82] at the interface between two solids with and without liquid films have been studied using the AFM and FFM. Surface roughness is routinely measured using the AFM[83–86], and both instruments have been used for measuring elastic–plastic mechanical properties[72,73,76,77,87–89]. At most solid–solid interfaces of technological relevance, contact occurs at numerous asperities[1,4,15,16]; a sharp AFM/FFM tip sliding on a surface simulates just one such contact[15,16]. For measurements of surface roughness, friction forces and nanoscale scratching and wear, a microfabricated square-pyramidal $Si_3N_4$ or silicon tip with a tip radius ranging from 10 to 50 nm is generally used[16] at loads ranging from 10 to 150 nN. For measurements of microscale scratching and wear, and for nanoindentation hardness measurements and nanofabrication, a three-sided pyramidal single-crystal natural-diamond tip with a tip radius of about 100 nm is generally used[16] at relatively high loads, ranging from 10 to 150 μN.

**Surface roughness, adhesion and friction.** Solid surfaces, irrespective of their method of formation, generally contain surface irregularities. When two nominally flat surfaces are placed in contact, surface roughness causes contact to occur at discrete contact points. Deformation occurs at these points, and may be either elastic or plastic, depending on the nominal stress, surface roughness and material properties. The sum of the areas of all the contact points constitutes the real area of contact, and for most materials at normal loads, this will be only a small fraction of the area that would be in contact if the surfaces were perfectly smooth. In general, this real area of contact must be minimized to minimize adhesion, friction and wear[1,2].

Characterizing surface roughness is therefore important for predicting and understanding the tribological properties of solids in contact. The AFM has been used to measure surface roughness on length scales from nanometres to micrometres[2,83–86]. Surface roughness most commonly refers to the variations in the height of the surface relative to a reference plane[1,2]. Commonly measured roughness parameters, such as r.m.s. surface height and peak-to-valley distance, are found to be scale-dependent for any given surface. The topography of most engineering surfaces is fractal, possessing a self-similar structure over a range of scales. By using fractal analysis one can characterize the roughness of such surfaces with two scale-independent fractal parameters $D$ and $C$, which provide information about roughness at all length scales[83–86]. These two parameters are instrument-independent and are unique for each surface. $D$ (generally ranging from 1 to 2) primarily relates to distribution of different frequencies in the surface profile, and $C$ to the amplitude of the surface height variations at all frequencies. A fractal model of elastic–plastic contacts[84] has been used to predict whether contacts experience elastic or plastic deformation, and to predict the statistical distribution of contact points.

To study friction mechanisms on an atomic scale, a well characterized, freshly cleaved surface of highly oriented pyrolytic graphite (HOPG) has been studied by Mate *et al.*[27] and Ruan and Bhushan[74]. The atomic-scale friction force of HOPG exhibited the same periodicity as the corresponding topography

(Fig. 3*a*), but the peaks in friction and those in topography were displaced relative to each other[74] (Fig. 3*b*). A Fourier expansion of the interatomic potential was used to calculate the conservative interatomic forces between atoms of the FFM tip and those of the graphite surface. Maxima in the interatomic forces in the normal and lateral directions do not occur at the same location, which explains the observed shift between the peaks in the lateral force and those in the corresponding topography. Furthermore, the observed local variations in friction force can be explained by variation in the intrinsic lateral force between the sample and the FFM tip[74], and these variations may not necessarily occur as a result of atomic-scale stick–slip processes[27,90,91].

Frictional forces of HOPG have also been studied on micrometre scales[70,75–77,92]. Local variations in the microscale friction of cleaved graphite are observed, which arise from structural changes that occur during the cleaving process[75]. The cleaved HOPG surface is largely atomically smooth but exhibits line-shaped regions in which the coefficient of friction is more than order of magnitude larger. Transmission electron microscopy indicates that the line-shaped regions consist of graphite planes of different orientation, as well as of amorphous carbon. Differences in friction can also be seen for organic mono- and multilayer films[70], which again seem to be the result of structural variations in the films. These measurements suggest that the FFM can be used for structural mapping of the surfaces. FFM measurements can be used to map chemical variations, as indicated by the use of the FFM with a modified probe tip to map the spatial arrangement of chemical functional groups in mixed organic monolayer films[92]. Here, sample regions that had stronger interactions with the functionalized probe tip exhibited larger friction.

Local variations in the microscale friction of scratched surfaces can be significant, and seen to depend on the local surface slope rather than the surface height distribution[16,71–77]. Directionality in friction is sometimes observed on the macroscale; on the microscale this is the norm[16,28,71–77]. This is because most 'engineering' surfaces have asymmetric surface asperities, so that the interaction of the FFM tip with the surface is dependent on the direction of the tip motion. Moreover, during surface finishing processes material can be transferred preferentially onto one side of the asperities, which also causes asymmetry and directional dependence. Reduction in local variations and in directionality of frictional properties therefore requires careful optimization of surface roughness distributions and of surface-finishing processes.

Table 1 shows the coefficients of friction measured for two surfaces on micro- and macroscales. The coefficient of friction

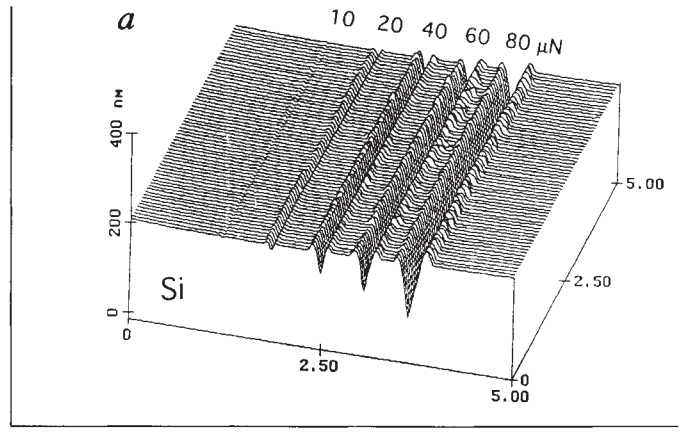


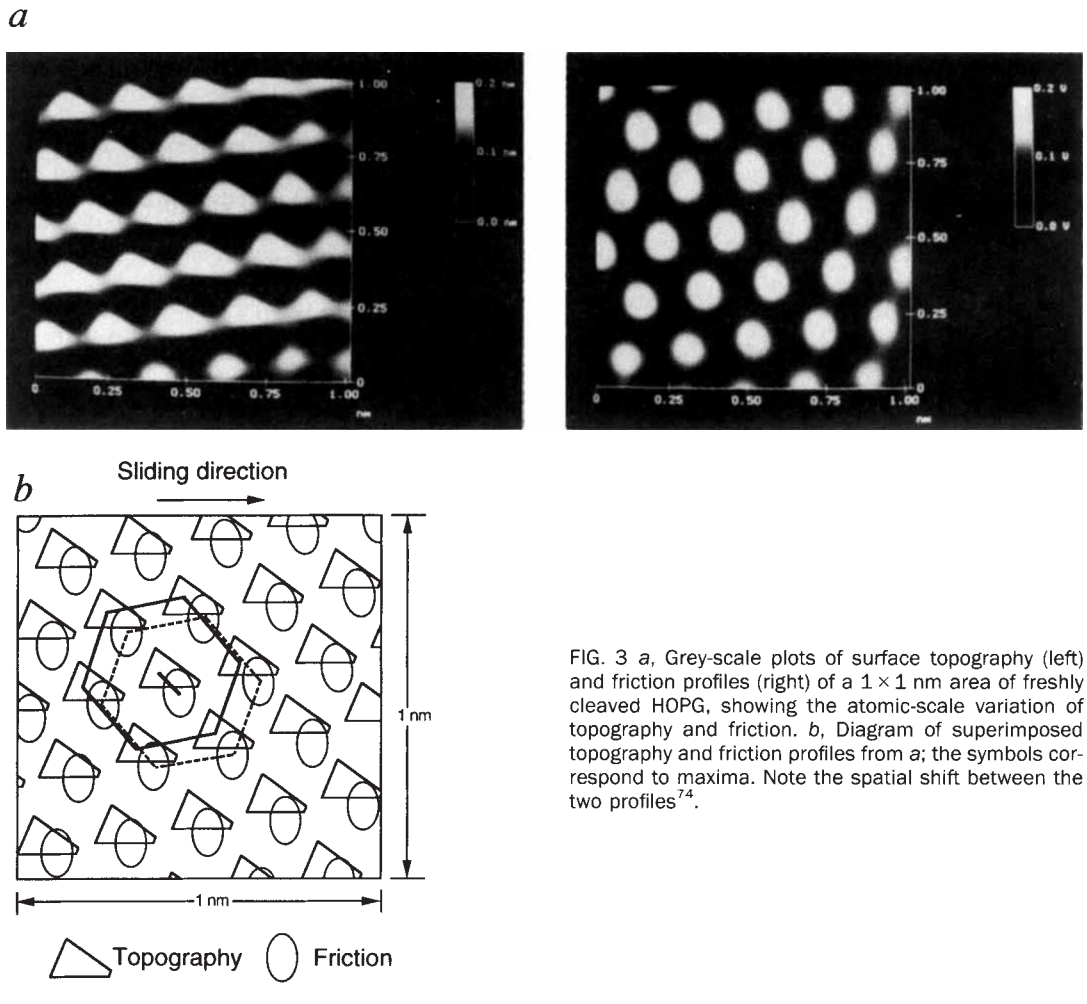


FIG. 3 *a*, Grey-scale plots of surface topography (left) and friction profiles (right) of a 1 × 1 nm area of freshly cleaved HOPG, showing the atomic-scale variation of topography and friction. *b*, Diagram of superimposed topography and friction profiles from *a*; the symbols correspond to maxima. Note the spatial shift between the two profiles[74].

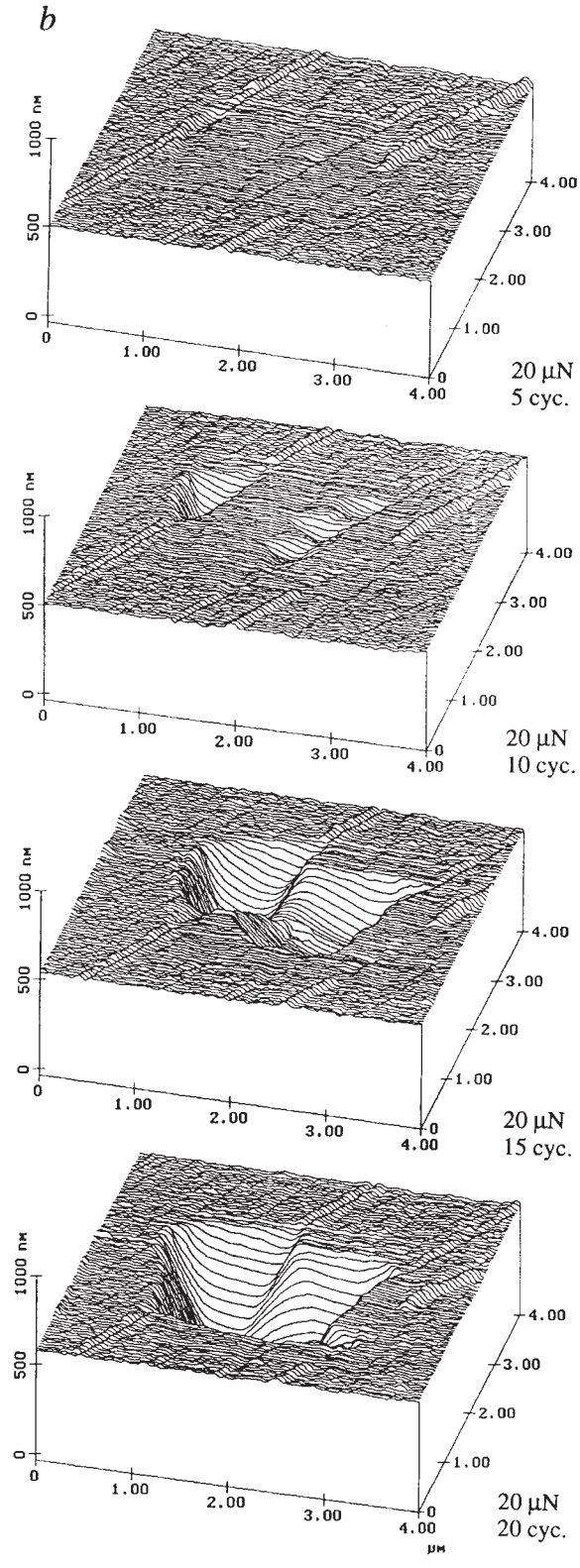


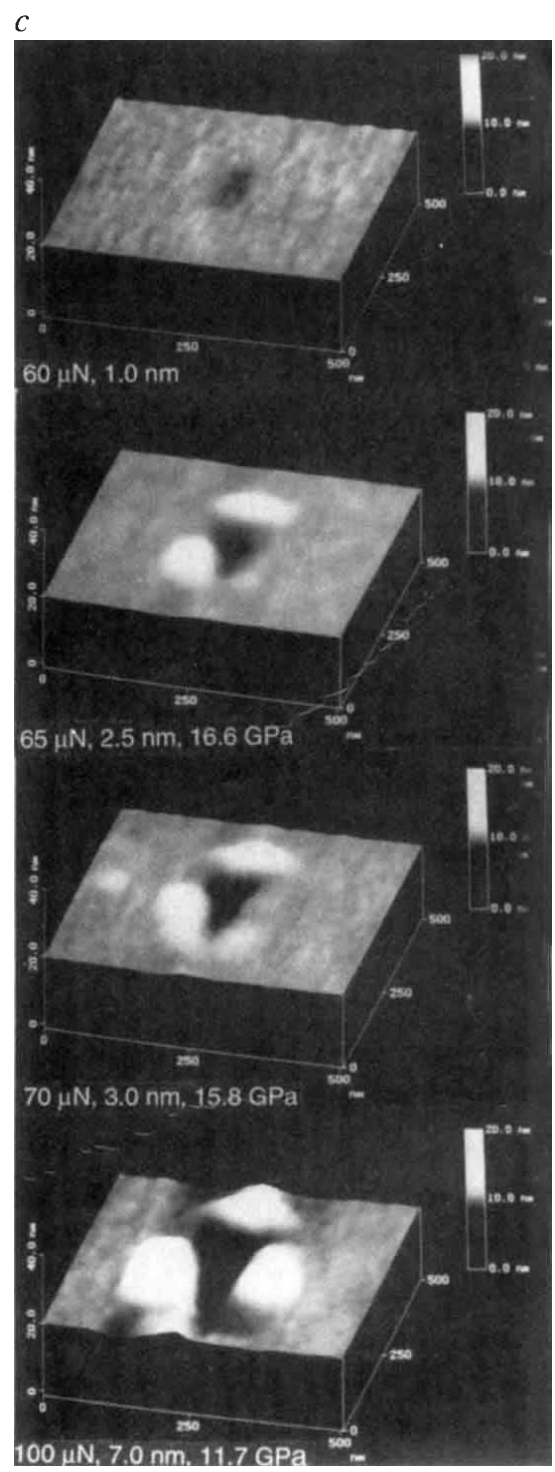


FIG. 4 *a*, Surface profile of Si(111) scratched at various loads[73]; note that the *x* and *y* axes are in μm, and the *z* axis in nm. *b*, Surface profiles of diamond-like carbon-coated thin-film disk showing the worn region; the normal load and the number of test cycles are indicated[72]. (Units of axes as in *a*.) *c*, Grey-scale plots of images of indentation marks on the Si(111) samples; loads, indentation depths and hardness values are indicated[89]. (All axes in nm.)

is defined as the ratio of the friction force to the normal load. The values on the microscale are much lower than those on the macroscale. When measured for the small contact areas and very low loads used in microscale studies, indentation hardness and modulus of elasticity are higher than at the macroscale. This reduces the degree of wear. In addition, the small apparent areas of contact reduce the number of particles trapped at the interface, and thus minimize the 'ploughing' contribution to the friction force.

At higher loads, however, the coefficient of friction for microscale measurements increases towards values comparable with those obtained from macroscale measurements, and surface

TABLE 1 Surface roughness and coefficients of friction

| Material | r.m.s. roughness (nm) | Micro-scale coefficient of friction versus $Si_3N_4$ tip* | Macro-scale coefficient of friction versus alumina ball† |
|---|---|---|---|
| Si(111) | 0.11 | 0.03 | 0.18 |
| $C^+$-implanted Si | 0.33 | 0.02 | 0.18 |

Data from refs 73 and 81.

* Tip radius of ~50 nm in the load range 10–150 nN (2.5–6.1 GPa), a scanning speed of 5 μm $s^{-1}$ and scan area of 1 × 1 μm.

† Ball radius of 3 mm at a normal load of 0.1 N (0.3 GPa) and average sliding speed of 0.8 mm $s^{-1}$.

damage also increases. Thus Amontons' law of friction[1,2], which states that the coefficient of friction is independent of apparent contact area and normal load, does not hold for microscale measurements. These findings suggest that microcomponents sliding under lightly loaded conditions should experience very low friction and near-zero wear.

**Scratching, wear and indentation.** The AFM can be used to investigate how surface materials may be moved or removed on micro- to nanoscales, for example through scratching and wear[71–73,76–78] (where these things are undesirable), and nanomachining and nanofabrication (where they are desirable). The AFM can also be used for measurements of mechanical properties on micro- to nanoscales. Figure 4*a* shows microscratches made on Si(111) at various loads after 10 cycles. As expected, the depth of scratch increases with load. Such microscratching measurements can be used to study failure mechanisms on the microscale and to evaluate the mechanical integrity (scratch resistance) of ultra-thin films at low loads[71,72].

By scanning the sample in two dimensions with the AFM, wear scars are generated on the surface. The evolution of wear of a diamond-like carbon coating on a polished aluminium substrate is shown in Fig. 4*b*, which illustrates how the micro-wear profile for a load of 20 μN develops as a function of the number of scanning cycles[72]. Wear is not uniform, but is initiated at nanoscratches, indicating that surface defects (with high surface energy) act as initiation sites. Thus, scratch-free surfaces will be relatively resistant to wear.

Mechanical properties, such as hardness and modulus of elasticity can be determined on micro- to picoscales using the AFM[72,73,76,77,87–89]. Indentability on the scale of picometres can be studied by monitoring the slope of cantilever deflection as a function of sample travelling distance after the tip is engaged and the sample is pushed against the tip[71]. For a rigid sample, the cantilever deflection is the same as the sample travelling distance; but the former quantity is smaller if the tip indents the sample. The indentation hardness of surface films with an indentation depth as small as 1 nm has been measured for Si(111)[89] (Fig. 4*c*). Triangular indentations are observed for shallow penetration depths. The hardness for an indentation depth of 2.5 nm is 16.6 GPa; it drops to 11.7 GPa at a depth of 7 nm. This decrease in hardness with increase in indentation depth can be rationalized on the basis that as the volume of deformed material increases, there is a higher probability of encountering material defects[93]. Bhushan and Koinkar[73] have used AFM measurements to show that ion implantation of silicon surfaces increases their hardness and thus their wear resistance. Formation of surface alloy films with improved mechanical properties by ion implantation is of growing technological importance as a means of improving the mechanical properties of materials.

The Young's modulus of elasticity is calculated from the slope of the indentation curve during unloading[16,87]. Maivald *et al.*[88] used an AFM in 'force modulation mode' to measure surface elasticities: the AFM tip is scanned over the modulated sample surface with the feedback loop keeping the average force constant. For the same applied force, a soft area deforms more, and thus causes less cantilever deflection, than a hard area. The ratio of modulation amplitude to the local tip deflection is then used to create a 'force modulation image'. The force modulation mode makes it easier to identify soft areas on hard substrates.

Detection of the transfer of material on a nanoscale is possible with the AFM. Indentation of $C_{60}$-rich fullerene films with an AFM tip has been shown[94] to result in the transfer of fullerene molecules to the AFM tip, as indicated by discontinuities in cantilever deflection as a function of sample travelling distance in subsequent indentation studies.

**Boundary lubrication.** The 'classical' approach to lubrication uses freely supported multimolecular layers of liquid lubricants[64,79,80]. But for lubrication of microdevices, a more effective approach involves the deposition of organized, dense molecular layers of long-chain molecules on the surfaces in contact. Such monolayers and thin films are commonly produced by Langmuir–Blodgett (LB) deposition and by chemical grafting of molecules into self-assembled monolayers (SAMs)[81]. All of these approaches involve boundary lubrication. The AFM and FFM have been used to study the lubricating effects of freely supported, LB and SAM films[81,82]. For freely supported liquid lubricants, either increasing the film thickness or chemically

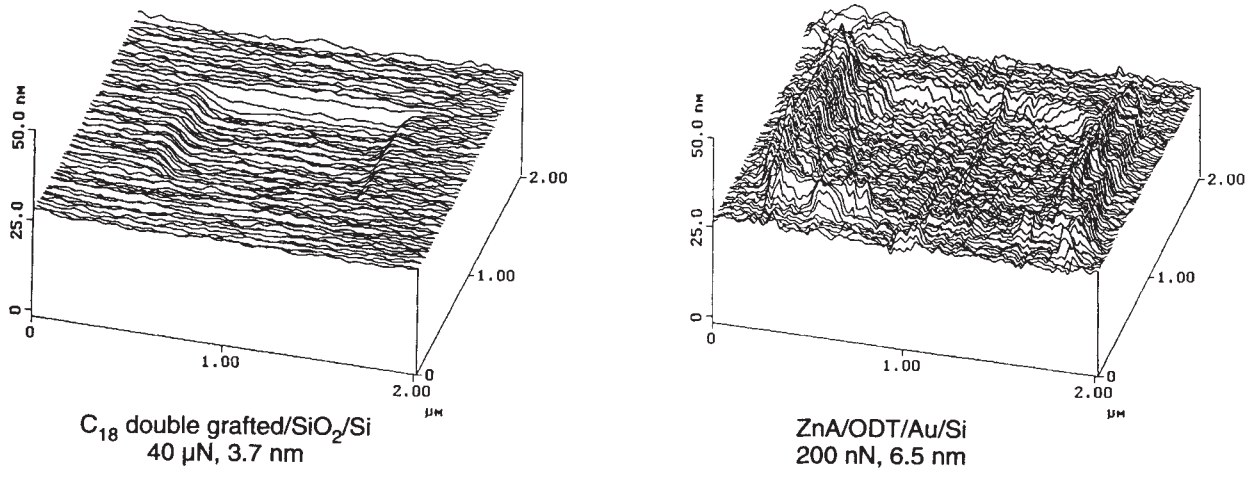


FIG. 5 Surface profiles showing the worn region after one scan cycle for self-assembled monolayers of octodecyl silanol (left) and zinc arachidate (right). Normal force and the wear depths are indicated. Note that wear or ZnA film occurs at only 200 nN as compared to 40 μN for $C_{18}$ film[81].

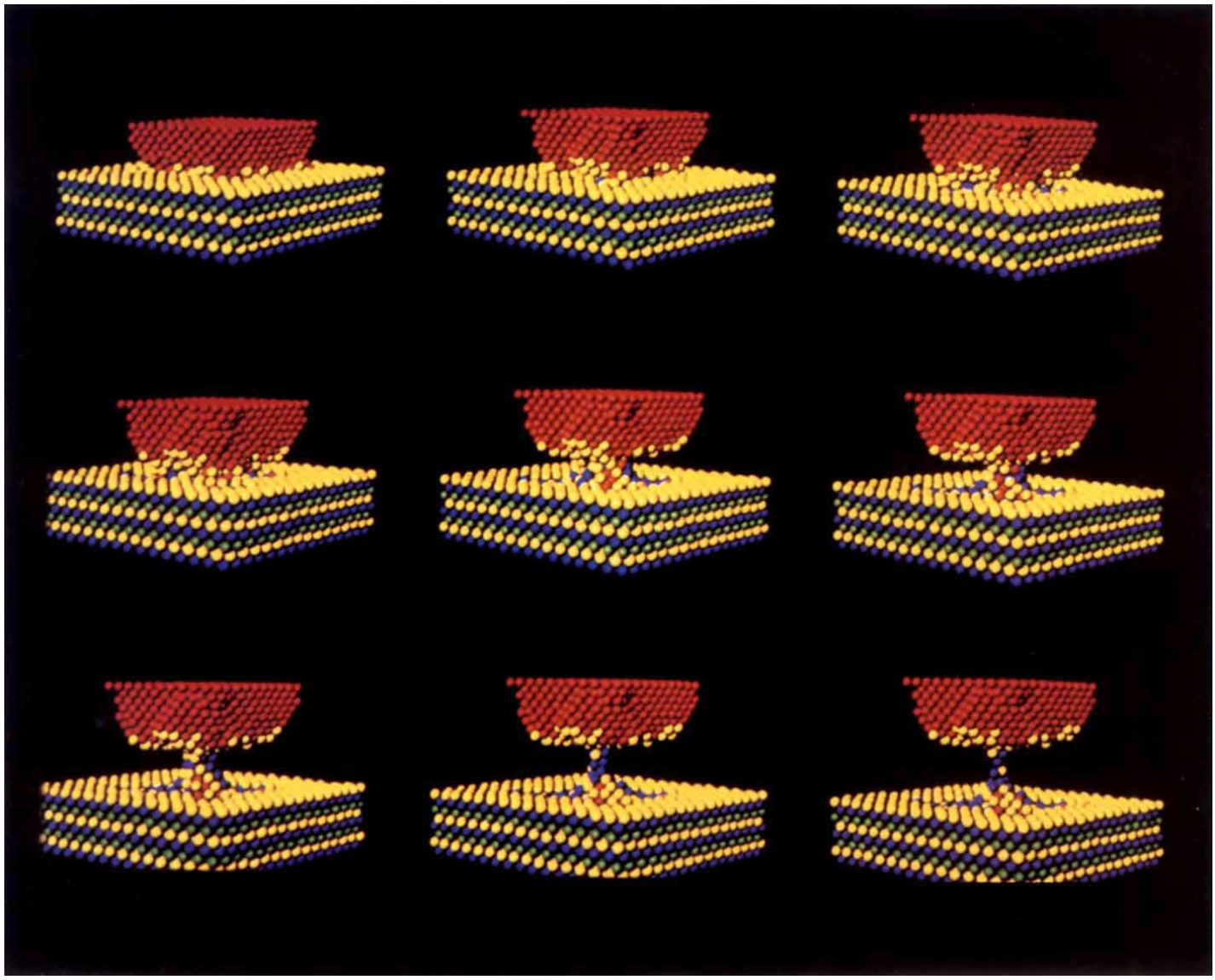

FIG. 6 Sequence of atomic configuration starting from a Ni tip indented in an Au(001) substrate (top left) and during the process of retraction of the tip (from left to right) accompanied by formation of a connective solid gold junction (bottom right). Red balls represent tip nickel atoms.

bonding the molecules to the substrate improves the lubrication performance[82]. SAMs of octodecyl ($C_{18}$) compounds based on aminosilanes on an oxidized silicon surface exhibit a lower coefficient of friction (0.018) and greater durability than LB films of zinc arachidate adsorbed on a gold surface coated with octadecylthiol (ODT) (coefficient of friction, 0.03) (Fig. 5)[81]. LB films are bonded to the substrate only by weak van der Waals attraction, whereas SAMs are chemically bound via covalent bonds. Because of the choice of chain length and terminal linking group that SAMs offer, they hold great promise for boundary lubrication of microdevices.

Measurements of the thickness of ultra-thin lubricant films with nanometre lateral resolution can be made with the AFM[95–97]. The lubricant thickness is obtained by measuring the force on the tip as it approaches, contacts and pushes through the liquid film and ultimately contacts the substrate. The distance between the sharp 'snap-in' (owing to the formation of a liquid meniscus between the film and the tip) at the liquid surface and the hard repulsion at the substrate surface is a measure of the liquid film thickness. This technique is now used routinely in the information-storage industry for thickness measurements (with nanoscale spatial resolution) of lubricant films, a few nanometres thick, in rigid magnetic disks.

## Atomic-scale simulations

An understanding of tribological phenomena at the molecular scale requires the non-trivial task of unravelling the energetics, structure, dynamics and transport processes of non-uniform systems involving a whole host of materials (metals, ionic solids, semiconductors, ceramics, organic and polymeric materials), under nonequilibrium conditions and often beyond the linear-response regimes for mechanical and flow behaviour. Consequently, until rather recently, most theoretical approaches to tribological problems have been anchored in continuum formulations, which assume continuous materials properties and use the formalisms of contact mechanics, hydrodynamics, viscous flow and elastohydrodynamics. But advances in theoretical understanding of the nature of interatomic interactions in materials, combined with the development of methods for computer-based modelling of complex many-body systems, have now opened up new avenues for exploring the properties of materials at high spatial and temporal resolution[98]. These studies employ

large-scale molecular-dynamics simulations, in which the trajectories in phase space of systems consisting of thousands of atoms (and subject to appropriate boundary conditions) are calculated from the particles' newtonian equations of motion. Generally the nature of the many-body interactions are derived from quantum-mechanical calculations. Analyses of particle trajectories allow the determination of structural, energetic, dynamical and mechanical properties of the system on nanometre distance scales and femtosecond timescales. Some of the results obtained from such simulations correlate well with the predictions of theories constructed on the basis of macroscopic considerations[35,99]. Thus these results help to elucidate the microscopic origin of the macroscopic behaviour.

On the other hand, as we have seen to be the case experimentally, simulations often reveal that the physical behaviour of materials at interfaces can be very different from that in the bulk. These interface-specific phenomena include atomic-scale adhesion and interfacial wetting on contact formation[66,99], generation of atomic-scale connective wires by the separation of metal–metal contacts[66,100], atomic-scale stick–slip friction[56,90,91] and structural ordering and phase transitions in thin lubricant films pressed and sheared between confining solid plates[46,58,60,101]. Some of these effects are quite general to systems confined to molecular dimensions in one or more directions, and they may determine the range of validity of macroscopic descriptions of the mechanical, rheological and flow properties of materials. Atomic-scale simulations can be of great value for interpreting the results of micro- and nanotribological experiments, particularly those involving scanning-probe microscopies, the surface-force apparatus and microbalance techniques. Moreover, understanding the behaviour of materials of very small dimensions is relevant to the development of nano- and microfabricated devices and to the atomic-scale manipulation of materials[98,102].

**Interfacial solid junctions.** Attempts to understand the key issue in friction—the origins and nature of excitations, and the transfer and dissipation of energy occurring when two bodies slide in contact—date back several centuries[103]. For metals, the current view (which emerged over four decades ago) is that the friction force is essentially the force required to shear intermetallic junctions formed at the regions of real contact, plus the force required to plough the surface of the softer material by the asperities of the harder[1].

Simulations of a clean gold substrate contacted by a nickel tapered and faceted tip, and for the reverse situation of a nickel surface and a gold tip, revealed[66,100] the onset of an instability as the tip approaches the sample to a distance of about 4 Å. At this point there occurs a jump to contact (with gold atoms being displaced by about 2 Å in about 1 picosecond), with adhesive bonding between the two materials driven and accompanied by atomic-scale wetting of nickel by gold atoms. The latter is the result of differences in their surface energies, just as it is for the case of surface wetting by a liquid film. Retraction of the tip from the surface after contact causes significant inelastic deformation of the sample, involving ductile extension, formation of a connective neck of atomic dimensions, and eventual rupture. The final result on separation is a gold-coated nickel tip and a damaged gold surface. These phenomena, which were observed also in simulations in which the tip penetrated the surface, involve transitions from elastic to plastic behaviour of the metals. The formation of an extended, atomically thin crystalline connective wire (Fig. 6) gives rise to marked hysteresis in the force–distance relation between the materials on lowering and lifting the tip. The elongation of the crystalline junction exhibits straining and yielding stages, with a periodicity equal to that of the interlayer spacing in the wire, which is reflected in periodic oscillations in the recorded force. This behaviour has been seen experimentally in AFM studies of solid junctions[66], and also in room temperature STM measurements of the electrical conductance of atomically thin gold wires up to 50 Å long[104,105] formed between the tip and a gold surface, exhibit a periodic quantization in units of the conductance quantum ($2e^2/h$, where $e$ is the electron charge and $h$ is Planck's constant). For longer wires, of lengths greater than 100 Å, the onset of localization was observed[10].

Simulations of the interactions between the surfaces of crystalline ionic solids ($CaF_2$)[56] and between semiconductor surfaces (silicon)[90,91] exhibit similar jumps to contact and force hysteresis. Ionic solids are less easily deformed plastically, however; rather,

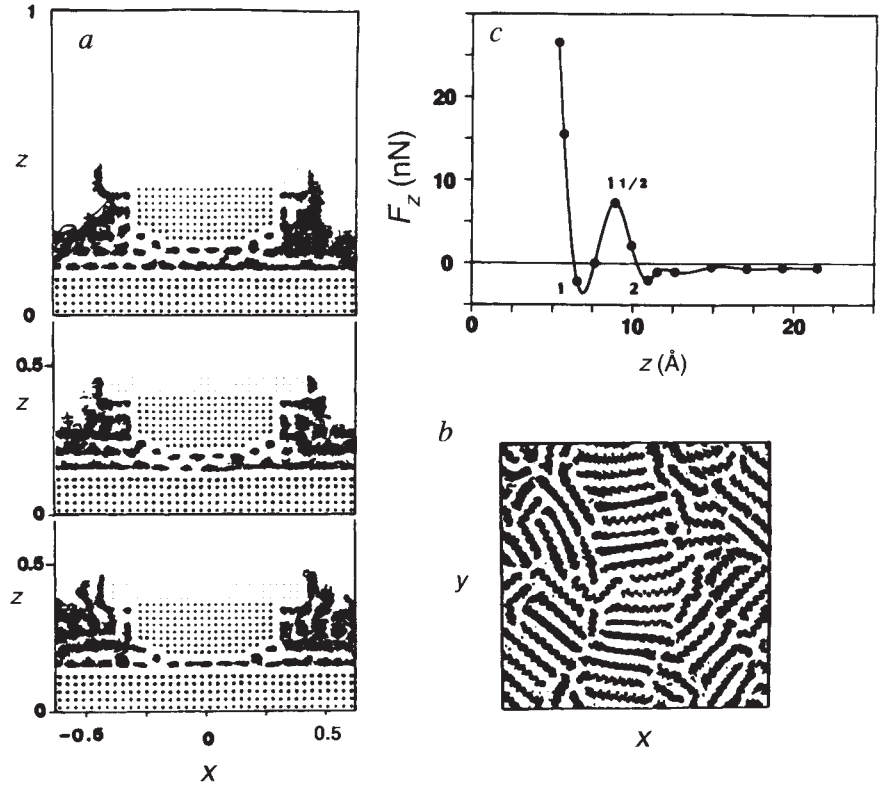


FIG. 7 *a*, Side views of atomic configurations of a nickel tip, an Au(001) surface and an *n*-$C_{16}H_{34}$ (hexadecane) film, starting at a tip-to-surface spacing corresponding to two layers of the confined film ($d_{ts}$ = 11 Å, top) and ending with a one-layer film ($d_{ts}$ = 6.5 Å, bottom). The middle configuration corresponds to spacing $d_{ts}$ = 9 Å. The linear dimension of the system along the *x* axis is 77.5 Å, and the configurations were obtained in a vertical slice in the *xz* plane of a width of 16 Å. In this figure, the coordinate axes are normalized such that $x = z = 1$ corresponds to a linear dimension of 77.5 Å. *b*, Short-time trajectories of hexadecane molecules in the layer next to the Au(001) surface, corresponding to the one-layer confined film shown at the bottom of *a*, illustrating intra-layer ordered domains. (The linear dimension of the system along the *x* and *y* axes is 77.5 Å.) *c*, Normal force on the nickel tip versus the distance between the tip and the gold surface, *z*, recorded during the process of lowering of the nickel tip onto the hexadecane-covered Au(001) surface, and illustrating force oscillations associated with the layering transformations in the film.

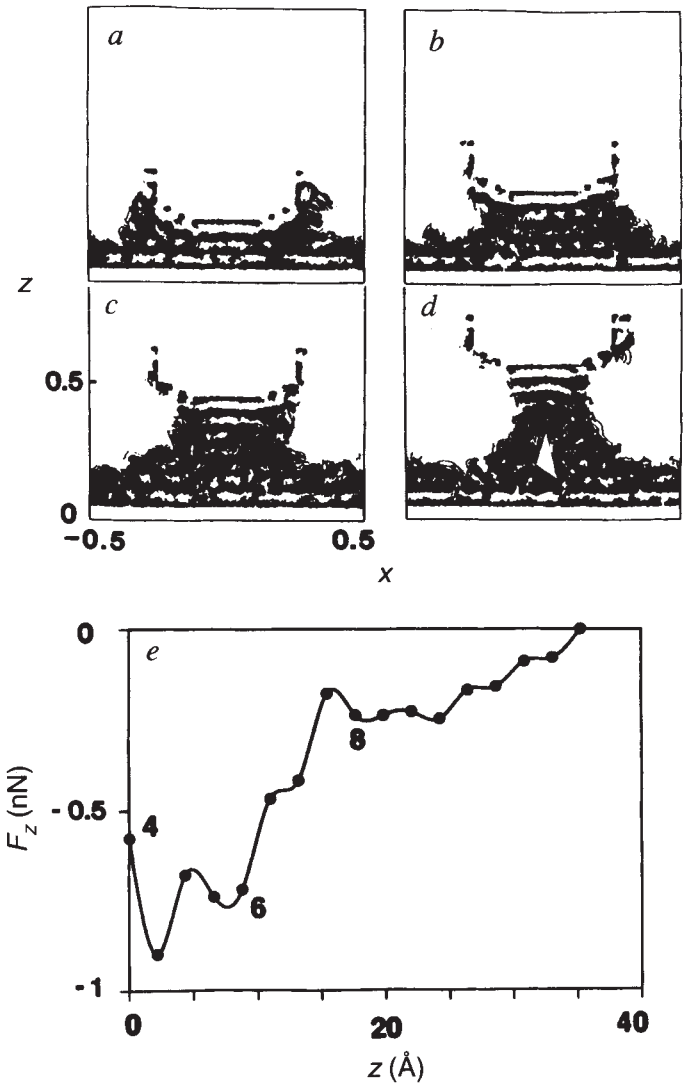


FIG. 8 *a–d*, Short-time trajectories, obtained from molecular-dynamics simulations, of hexadecane molecules at 350 K forming a capillary column between a gold substrate and a nickel tip at four stages of the tip-lifting process. Trajectories were plotted in a slice (23 Å wide) through the middle of the system. The distances (Å) between the tip and the substrate for the configurations shown in *a–d* are $d_{ts} = 19.3$, 28.1, 36.9 and 45.7 Å, respectively. The length scale of the calculational cell, which was periodically repeated along the *x* and *y* directions, is 77.5 Å. (In this figure, the coordinate axes are normalized such that $x = z = 1$ corresponds to a linear dimension of 77.5 Å.) *e*, The recorded normal force on the nickel tip ($F_z$) versus the distance between the tip and the gold surface, *z*, with the origin taken as that corresponding to a four-layer capillary column (see *a*). Dots indicate distances for which the system was relaxed during the tip lifting process. The numbers on the graph denote the number of layers in the capillary column (for the eight-layer column, the number is ambiguous due to disordering in the middle part, see *c*). The changes in the structural nature of the film on elongation of the capillary junction are reflected in the variation in $F_z$.

they tend to exhibit brittle failure. Such simulations of two materials in contact sliding with respect to one another revealed atomic-scale stick–slip behaviour (oscillatory bond forming and bond breaking)[90,91], shearing of the probe tip and interfacial material transfer[56], and fragmentation owing to asperity collisions[106]. Some of these results have been used to calculate the critical yield stress of sheared ionic interfaces and its temperature dependence; these predictions can again be tested against experiments.

Simulations of atomic-scale friction between diamond (111) surfaces (chosen because of the potential use of diamond as a low-friction wear-resistant coating) have revealed[107] the atomic-scale mechanisms of energy transfer between fully hydrogen- or methyl-terminated diamond surfaces. Energy transfer is relatively efficient, and thus the friction coefficients are relatively high. But the friction coefficient is reduced when longer hydrocarbons are chemisorbed to the surface. For low loads, this reduction can be ascribed to alignment of the molecules in the sliding direction; at high loads it is the result of diminished corrugation of the underlying surface, caused by the tendency of the chemisorbed molecules to occupy corrugation troughs.

**Interfacial liquid junctions and confined films.** Molecular-dynamics simulations of the nanotribology of interfacial liquids and confined films aim to explore the relation between the physical properties and response of model lubricants and their molecular characteristics, such as chain lengths and molecular structural complexity (for example, straight versus branched chains). Such simulations of alkanes and self-assembled boundary-lubricant systems have revealed liquid-junction formation[35,36], inhibition of the generation of solid junctions[56] layering phenomena and in-plane ordering owing to confinement[34–45], and have shown how self-assembled monolayers[42,108–110] respond to compression by a tip or flat surface. Simulations have also been performed of collapse and drainage mechanisms of confined molecular films and their dependence on the strength of bonding to the substrate[34], the dependence of thin-film viscosities on the shear rate[111] and the origin of stick–slip phenomena in shear-induced 'solidification' and melting[46,60,101], mechanisms of cavitation in thin molecular liquid films induced by fast motion of immersed tips[112], and correlations between structural and dynamical transformations in lubricating films with force–distance characteristics[35,36,112] (Figs 7 and 8). Simulations of thin-film model lubricants made of mixtures of long-chain molecules of different lengths have illuminated the molecular mechanism of preferential surface segregation of the longer-chain molecules[55].

These simulations have generally considered flat, atomically structured crystalline solids as the substrates. Some recent simulations, on the other hand, have modelled interactions between surface asperities for a sliding metallic contact lubricated by a thin (~20 Å) film of hexadecane[113]. These simulations are relevant to many technological problems, ranging from elastohydrodynamic lubrication of gears, rolling bearings and cam-followers, to tribology in future generations of information-storage devices[2,4]. For relative sliding velocities in the range 10–20 m $s^{-1}$, spatial and temporal variations in the density of the lubricant, particularly in the region between the approaching asperities can lead to glassification and seizure of the contact. In addition, sliding asperity contacts can induce dynamical structural layering of the lubricant resulting in oscillatory behaviour of the friction forces and ultimately breakdown of the lubricant film, up to the molecular level, accompanied by trapping of molecules in the space between the two asperities. The asperities themselves can be deformed markedly, leading to the formation of metal–metal junctions and transfer of material between the surfaces. Cavitation was observed in the region between two departing asperities following collision. Such simulations extend investigations of elastohydrodynamic lubrication to the nanoscale domain, which is beyond the range of applicability of continuum models[114–116].

## Concluding remarks

These theoretical and experimental studies of tribology at the molecular scale have not just extended, but in some cases fundamentally altered, the picture that had developed from macroscale studies. For example, the traditional picture of stick–slip motion ascribed it to a negative slope in the friction–velocity function[1,2], but recent work has put this in reverse: in many cases stick–slip behaviour is seen to be the primary process—arising from successive freezing and melting transitions of the shearing film—and it is this that gives rise to the negative friction–velocity

dependence[46]. SFA experiments on films of complex fluids and polymers have also shown why branched-chain molecules are better lubricants than straight-chain molecules, even though the former have much higher bulk viscosities: the symmetrically shaped straight-chain molecules are prone to ordering and freezing, which dramatically increases their resistance to shear, whereas the irregularly shaped, branched molecules remain in the liquid state even under high loads. Straight-chain molecules, however, make ideal clutch fluids, for which high friction is required.

Investigations of wear, scratching and indentation on nanoscales using the AFM can provide insights into failure mechanisms of materials. Coefficients of friction, wear rates and mechanical properties such as hardness have been found to be different on the nanoscale than on the macroscale: generally, coefficients of friction and wear rates on micro- and nanoscales are smaller, whereas hardness is greater.

As the trend towards miniaturization of technological devices continues, these studies indicate that very small micromechanical machines may behave in ways that cannot be predicted from their larger counterparts. It is encouraging in this regard to find that materials properties at small scales can be superior—wear is lower, friction less. Moreover, new lubrication strategies such as the use of self-assembled monolayers promise to be very versatile and effective at these scales. On the other hand, phenomena such as shear-induced solidification and the formation of bridges between contact asperities indicate that the nanotribological regime poses novel challenges of its own. □

*B. Bhushan is at the Computer Microtribology and Contamination Laboratory, 206 West 18th Avenue, The Ohio State University, Columbus, Ohio 43210-1107, USA. J. N. Israelachvili is at the Department of Chemical and Nuclear Engineering, University of California, Santa Barbara, California 93106, USA. U. Landman is at the School of Physics, Georgia Institute of Technology, Atlanta, Georgia 30332, USA.*


1. Bowden, F. P. & Tabor, D. *The Friction and Lubrication of Solids* Parts I & II (Clarendon, Oxford, 1950 & 1964).
2. Bhushan, B. *Tribology and Mechanics of Magnetic Storage Devices* (Springer, New York, 1990).
3. Bhushan, B. & Gupta, B. K. *Handbook of Tribology: Materials, Coatings and Surface Treatments* (McGraw-Hill, New York, 1991).
4. Bhushan, B. *Mechanics and Reliability of Flexible Magnetic Media* (Springer, New York, 1992).
5. Gane, N. & Bowden, F. P. *J. appl. Phys.* **39,** 1432–1435 (1968).
6. Skinner, J. & Gane, N. *J. Phys.* D**5,** 2087–2094 (1972).
7. Pollock, H. M., Shufflebottom, P. & Skinner, *J. J. Phys.* D**10,** 127–138 (1977).
8. Maugis, D., Desatos-Andarelli, G., Heurtel, A. & Courtel, R. *Am. Soc. Lubrication Engrs* **21,** 1–19 (1978).
9. Pollock, H. M. *J. Phys.* D**11,** 39–54 (1978).
10. Pashley, M. D., Pethica, J. B. & Tabor, D. *Wear* **100,** 7–31 (1984).
11. Maugis, D. & Pollock, H. M. *Acta metall.* **32,** 1323–1334 (1984).
12. Pethica, J. B. *Phys. Rev. Lett.* **57,** 3235 (1986).
13. Pethica, J. B. & Oliver, W. C. *Physica Scripta* T**19,** 61–66 (1987).
14. Guo, Q., Ross, J. D. J. & Pollock, H. M. *Mater. Res. Soc. Proc.* **140,** 51–66 (1989).
15. *Fundamentals of Friction: Macroscopic and Microscopic Processes* (eds Singer, J. L. & Pollock, H. M.) (Kluwer, Dordrecht, 1991).
16. *Handbook of Micro/Nanotribology* (ed. Bhushan, B.) (CRC, Boca Raton, Florida, 1995).
17. Tabor, D. & Winterton, R. *Proc. R. Soc.* A**312,** 435–450 (1969).
18. Israelachvili, J. N. & Tabor, D. *Nature* **241,** 148–149 (1973); *Wear* **24,** 386–390 (1973).
19. Israelachvili, J. N. *Chemtracts—Analyt. phys. Chem.* **1,** 1–12 (1989).
20. Briscoe, B. J., Evans, D. C. & Tabor, D. *J. Colloid Interface Sci.* **61,** 9–13 (1977).
21. Israelachvili, J. N., Homola, A. M. & McGuiggan, P. M. *Science* **240,** 189–191 (1988).
22. Hirz, S. J., Homola, A. M., Hadziioannou, G. & Franc, C. W. *Langmuir* **8,** 328–333 (1992).
23. Granick, S. *Science* **253,** 1374–1379 (1991).
24. Klein, J., Perahia, D. & Warburg, S. *Nature* **352,** 143–145 (1991).
25. Binnig, G., Rohrer, H., Gerber, Ch. & Weibel, E. *Phys. Rev. Lett.* **49,** 57–61 (1982).
26. Binnig, G., Quate, C. F. & Gerber, Ch. *Phys. Rev. Lett.* **56,** 930–933 (1986).
27. Mate, C. M., McClelland, G. M., Erlandsson, R. & Chiang, S. *Phys. Rev. Lett.* **59,** 1942–1945 (1987).
28. Meyer, G. & Amer, N. M. *Appl. Phys. Lett.* **57,** 2089–2091 (1990).
29. Krim, J., Solina, D. H. & Chiarello, R. *Phys. Rev. Lett.* **66,** 181–184 (1991).
30. Christenson, H. K. *Chem. Phys. Lett.* **118,** 455–458 (1985); *J. phys. Chem.* **90,** 4–6 (1986).
31. Gee, M. L. & Israelachvili, J. N. *J. chem. Soc., Faraday Trans.* **86,** 4049–4058 (1990).
32. McGuiggan, P. M. & Israelachvili, J. N. *J. Mater. Res.* **5,** 2232–2243 (1990).
33. Israelachvili, J. N. *Acc. chem. Res.* **20,** 415–421 (1987).
34. Ribarsky, M. W. & Landman, U. *J. chem. Phys.* **97,** 1937–1949 (1992).
35. Luedtke, W. D. & Landman, U. *Comput. Mater. Sci.* **1,** 1–24 (1992).
36. Landman, U., Luedtke, W. D., Ouyang, J. & Xia, T. K. *Jap. J. appl. Phys.* **32,** 1444–1462 (1993).
37. Rhykerd, C., Schoen, M., Diester, D. & Cushman, J. *Nature* **330,** 461–463 (1987).
38. Schoen, M., Diestler, D. & Cushman, J. *J. chem. Phys.* **87,** 5464 (1987); *Phys. Rev.* B**47,** 5603–5613 (1987).
39. Diestler, D., Schoen, M. & Cushman, J. *Science* **262,** 545–547 (1993).
40. Han, K. K., Cushman, J. H. & Diestler, D. J. *Molec. Phys.* **79,** 537–545 (1993).
41. Schoen, M., Rhykerd, C., Diestler, D. & Cushman, J. *Science* **245,** 1223–1225 (1989).
42. Callaway, M., Tildesley, D. J. & Quirke, N. *Langmuir* **10,** 3350–3356 (1994).
43. Wang, Y., Hill, K. & Harris, J. G. *J. chem. Phys.* **100,** 3276–3285 (1994).
44. Kirk Hill, Y. W. & Harris, J. G. *Langmuir* **9,** 1983–1985 (1993).
45. Gupta, S., Koopman, D. C., Westerman-Clark, G. B. & Bitsanis, I. A. *J. chem. Phys.* **100,** 8444–8453 (1994).
46. Thompson, P. A. & Robbins, M. O. *Science* **250,** 792–794 (1990).
47. Israelachvili, J. N. *et al. J. Phys.: Condensed Matter* **2,** SA89–SA98 (1990).
48. Yoshizawa, H. & Israelachvili, J. *J. phys. Chem.* **97,** 11300–11313 (1993).
49. Van Alsten, J. & Granick, S. *Phys. Rev. Lett.* **61,** 2570–2573 (1988).
50. Hu, H. W., Carson, G. & Granick, S. *Phys. Rev. Lett.* **66,** 2758–2761 (1991).
51. Reiter, G., Demirel, A. L. & Granick, S. *Science* **263,** 1741–1744 (1994).
52. Xia, T. K., Ouyang, J., Ribarsky, M. W. & Landman, U. *Phys. Rev. Lett.* **69,** 1967–1970 (1992).
53. Xia, T. K. & Landman, U. *Phys. Rev.* B**48,** 11313–11314 (1993).
54. Xia, T. K. & Landman, U. *J. chem. Phys.* **101,** 2498–2507 (1994).
55. Xia, T. K. & Landman, U. *Science* **261,** 1310–1312 (1993).
56. Landman, U., Luedtke, W. D. & Ringer, E. M. *Wear* **153,** 3–30 (1992).
57. Homola, A. M., Israelachvili, J. N., Gee, M. L. & McGuiggan, P. M. *ASME J. Tribology* **111,** 675–682 (1989).
58. Robbins, M. O. & Thompson, P. A. *Science* **253,** 916 (1991).
59. Gee, M. L., McGuiggan, P. M., Israelachvili, J. N. & Homola, A. *J. chem. Phys.* **93,** 1895–1906 (1990).
60. Persson, B. N. J. *Phys. Rev.* B**50,** 4771–4786 (1994).
61. Yoshizawa, H., Chen, Y. L. & Israelachvili, J. *J. phys. Chem.* **97,** 4128–4140 (1993); *J. Adhesion Sci. Technol.* **8,** 1–18 (1994).
62. Yoshizawa, H., McGuiggan, P. & Israelachvili, J. N. *Science* **259,** 1305–1308 (1993).
63. Klein, J., Kumacheva, E., Mahalu, D., Perahia, D. & Fetters, L. J. *Nature* **370,** 634–636 (1994).
64. Blackman, G. S., Mate, C. M. & Philpott, M. R. *Phys. Rev. Lett.* **65,** 2270–2273 (1990).
65. Burnham, N. A., Domiguez, D. D., Mowery, R. L. & Colton, R. J. *Phys. Rev. Lett.* **64,** 1931–1934 (1990).
66. Landman, U., Luedtke, W. D., Burnham, N. A. & Colton, R. J. *Science* **248,** 454–461 (1990).
67. Ducker, W. A., Senden, T. J. & Pashley, R. M. *Langmuir* **8,** 1831–1836 (1992).
68. Salmeron, M. *et al. Langmuir* **9,** 3600–3611 (1993).
69. Kaneko, R., Miyamoto, T. & Hamada, E. *Adv. Info. Storage Syst.* **1,** 267–277 (1991).
70. Meyer, E. *et al. Thin Solid Films* **220,** 132–137 (1992).
71. Bhushan, B. & Ruan, J. *ASME J. Tribology* **116,** 389–396 (1994).
72. Bhushan, B., Koinkar, V. N. & Ruan, J. *Proc. Instn. Mech. Engrs.* J**208,** 17–29 (1994).
73. Bhushan, B. & Koinkar, V. N. *J. appl. Phys.* **75,** 5741–5746 (1994).
74. Ruan, J. & Bhushan, B. *J. appl. Phys.* **76,** 5022–5035 (1994).
75. Ruan, J. & Bhushan, B. *J. appl. Phys.* **76,** 8117–8120 (1994).
76. Bhushan, B. & Koinkar, V. N. *Tribology Trans.* **38,** 119–127 (1995).
77. Bhushan, B. & Koinkar, V. N. *Wear* **180,** 9–16 (1995); **183,** 360–370 (1995).
78. Miyamoto, T., Kaneko, R. & Miyake, S. *J. Vac. Sci. Technol.* B**9,** 1336–1339 (1991).
79. Mate, C. M. *Phys. Rev. Lett.* **68,** 3323–3326 (1992).
80. O'Shea, S. J., Welland, M. E. & Rayment, T. *Appl. Phys. Lett.* **61,** 2240–2242 (1992).
81. Bhushan, B. *et al. Langmuir* (in the press).
82. Bhushan, B., Miyamoto, T. & Koinkar, V. N. *Adv. Info. Storage Syst.* **6,** 151–161 (1995).
83. Majumdar, A. & Bhushan, B. *ASME J. Tribology* **112,** 205–216 (1990).
84. Majumdar, A. & Bhushan, B. *ASME J. Tribology* **113,** 1–11 (1991).
85. Bhushan, B. & Majumdar, A. *Wear* **153,** 53–64 (1992).
86. Ganti, S. & Bhushan, B. *Wear* **180,** 17–34 (1995).
87. Burnham, N. A. & Colton, R. J. *J. Vac. Sci. Technol.* A**7,** 2906–2913 (1989).
88. Maivald, P. *et al. Nanotechnology* **2,** 103–106 (1991).
89. Bhushan, B. & Koinkar, V. N. *Appl. Phys. Lett.* **64,** 1653–1655 (1994).
90. Landman, U., Luedtke, W. D. & Nitzan, A. *Surf. Sci.* **210,** L177–L184 (1989).
91. Landman, U., Luedtke, W. D. & Ribarsky, M. W. *J. Vac. Sci. Technol.* A**7,** 2829–2839 (1989).
92. Frisbie, C. D., Rozsnyai, L. F., Noy, A., Wrighton, M. S. & Lieber, C. M. *Science* **265,** 2071–2074 (1994).
93. Gane, N. & Cox, J. M. *Phil Mag.* **22,** 881–891 (1970).
94. Ruan, J. & Bhushan, B. *J. Mater. Res.* **8,** 3019–3022 (1993).
95. Mate, C. M., Lorenz, M. R. & Novotny, V. J. *J. chem. Phys.* **90,** 7550–7555 (1989).
96. Blackman, G. S., Mate, C. M. & Philpott, M. R. *Phys. Rev. Lett.* **65,** 2270–2273 (1990).
97. Bhushan, B. & Blackman, G. S. *ASME J. Tribology* **113,** 452–458 (1991).
98. Landman, U., Barnett, R. N., Cheng, H.-P., Cleveland, C. L. & Luedtke, W. D. in *Computations for the Nano-Scale* 75–113 (eds Bloohl, P. E., Joachim, C. & Fisher, A. J.) (Kluwer, Dordrecht, 1993).
99. Landman, U., Luedtke, W. D. & Ringer, E. M. in *Fundamentals of Friction: Macroscopic and Microscopic Processes* 463–508 (eds Singer, J. L. & Pollock, H. M.) (Kluwer, Dordrecht, 1991).
100. Landman, U. & Luedtke, W. D. *J. Vac. Sci. Technol.* **9,** 414–423 (1991).
101. Thompson, P. A., Robbins, M. O. & Grest, G. S. in *Computations for the Nano-Scale* 127–138 (eds Bloohl, P. E., Joachim, C. & Fisher, A. J.) (Kluwer, Dordrecht, 1993).
102. Luedtke, W. D. & Landman, U. *Phys. Rev. Lett.* **73,** 569–572 (1994).
103. Dowson, D. *History of Tribology* (Longman, London, 1979).
104. Pascual, J. I. *et al. Phys. Rev. Lett.* **71,** 1852–1855 (1993).
105. Pascual, J. I. *et al. Science* **267,** 1793–1795 (1995); *J. Vac. Sci. Technol.* (in the press).
106. Abraham, F. F., Rudge, W. E. & Alexopoulos, P. S. *Comput. mater. Sci.* **3,** 21–40 (1994).
107. Harrison, J. A., White, C. T., Colton, R. J. & Brenner, D. W. *Mater. Res. Soc. Bull.* **17,** 50–53 (1993).
108. Tupper, K. J., Colton, R. J. & Brenner, D. W. *Langmuir* **10,** 2041–2043 (1994).
109. Tupper, K. J. & Brenner, D. W. *Langmuir* **10,** 2335–2338 (1994).
110. Karaborni, S. *Phys. Rev. Lett.* **73,** 1668–1671 (1994).
111. Thompson, P. A., Grest, G. S. & Robbins, M. O. *Phys. Rev. Lett.* **68,** 3448–3451 (1992).
112. Landman, U. & Luedtke, W. D. *Mater. Res. Soc. Bull.* **17,** 36–44 (1993)
113. Gao, J., Luedtke, W. D. & Landman, U. *Science* (submitted).
114. Fowles, P. E., *J. Lub. Technol., Trans. ASME* **91,** 464–476 (1969).
115. Ai, X., Cheng, H. S. & Zheng, L., *ASME J. Tribology* **115,** 102–110 (1993).
116. Chang, L., Jackson, A. & Webster, M. N. *Tribology Trans.* **37,** 435–444 (1994).